

Ultralong continuously tunable parametric delays via a cascading discrete stage

Yitang Dai,^{1*} Yoshitomo Okawachi,¹ Amy C. Turner-Foster,² Michal Lipson,²
Alexander L. Gaeta,¹ and Chris Xu¹

¹*School of Applied and Engineering Physics, Cornell University, Ithaca, NY 14853, U.S.A.*

²*School of Electrical and Computer Engineering, Cornell University, Ithaca, NY 14853, U.S.A.*

* yd82@cornell.edu

Abstract: We report experimental demonstration of an all-optical continuously tunable delay line based on parametric mixing with a total delay range of 7.34 μ s. The bit-error rate performance of the delay line was characterized for a 10-Gb/s NRZ data channel. This result is enabled by cascading a discrete delay line that consists of 16 wavelength-dependent delays and a continuously tunable delay stage. Four wavelength conversion stages based on four-wave mixing in silicon waveguides were performed in order to achieve wavelength-preserving operation. The wavelength-optimized optical phase conjugation scheme employed in the delay line is capable of minimizing the residual dispersion for the entire tuning range.

©2009 Optical Society of America

OCIS codes: (190.4380) Nonlinear optics, four-wave mixing; (190.4390) Nonlinear optics, integrated optics.

References and links

1. R. Ramaswami, and K. N. Sivarajan, "Routing and wavelength assignment in all-optical networks," *IEEE/ACM Trans. Netw.* **3**(5), 489–500 (1995).
2. E. Choi, J. H. Na, S. Ryu, G. Mudhana, and B. H. Lee, "All-fiber variable optical delay line for applications in optical coherence tomography: feasibility study for a novel delay line," *Opt. Express* **13**(4), 1334–1345 (2005).
3. J. L. Corral, J. Marti, J. M. Fuster, and R. I. Laming, "True time-delay scheme for feeding optically controlled phased-array antennas using chirped-fiber gratings," *Photon. Technol. Lett.* **9**(11), 1529–1531 (1997).
4. G. N. Pearson, K. D. Ridley, and D. V. Willetts, "Chirp-pulse-compression three-dimensional lidar imager with fiber optics," *Appl. Opt.* **44**(2), 257–265 (2005).
5. Y. Han, and B. Jalali, "Photonic time-stretched analog-to-digital converter: Fundamental concepts and practical considerations," *J. Lightwave Technol.* **21**(12), 3085–3103 (2003).
6. R. Ramaswami, and K. N. Sivarajan, *Optical Networks: A Practical Perspective* (Morgan Kaufmann, 2002).
7. S. J. B. Yoo, "Optical packet and burst switching technologies for the future photonic internet," *J. Lightwave Technol.* **24**(12), 4468–4492 (2006).
8. R. W. Boyd, and D. J. Gauthier, "'Slow' and 'fast' light," *Progress in Optics*, vol. **43**, edited by E. Wolf (Elsevier, Amsterdam, 2002), Chap. 6, p. 497–530.
9. R. W. Boyd, D. J. Gauthier, and A. L. Gaeta, "Applications of slow light in telecommunications," *Opt. Photon. News* **17**(4), 18–22 (2006).
10. J. van Howe, and C. Xu, "Ultrafast optical delay line by use of a time-prism pair," *Opt. Lett.* **30**(1), 99–101 (2005).
11. J. E. Sharping, Y. Okawachi, J. van Howe, C. Xu, Y. Wang, A. E. Willner, and A. L. Gaeta, "All-optical, wavelength and bandwidth preserving, pulse delay based on parametric wavelength conversion and dispersion," *Opt. Express* **13**(20), 7872–7877 (2005).
12. J. Ren, N. Alic, E. Myslivets, R. E. Saperstein, C. J. McKinstrie, R. M. Jopson, A. H. Gnauck, P. A. Andrekson, and S. Radic, "12.47 ns continuously-tunable two-pump parametric delay," *ECOC 2006, Th4.4.3 PDP*.
13. Y. Wang, C. Yu, L. Yan, A. E. Willner, R. Roussev, C. Langrock, M. M. Fejer, J. E. Sharping, and A. L. Gaeta, "44-ns continuously tunable dispersionless optical delay element using a PPLN waveguide with two-pump configuration, DCF, and a dispersion compensator," *Photon. Technol. Lett.* **19**(11), 861–863 (2007).
14. Y. Okawachi, M. A. Foster, X. Chen, A. C. Turner-Foster, R. Salem, M. Lipson, C. Xu, and A. L. Gaeta, "Large tunable delays using parametric mixing and phase conjugation in Si nanowaveguides," *Opt. Express* **16**(14), 10349–10357 (2008).
15. E. Myslivets, N. Alic, J. R. Windmiller, R. M. Jopson, and S. Radic, "400 ns continuously tunable delay of 10 Gbps intensity modulated optical signal," *Photon. Technol. Lett.* **21**(4), 251–253 (2009).
16. L. C. Christen, O. F. Yilmaz, S. R. Nuccio, X. Wu, I. Fazal, A. E. Willner, C. Langrock, and M. M. Fejer, "Tunable 105 ns optical delay for 80 Gb/s RZ-DQPSK, 40 Gb/s RZ-DPSK, and 40 Gb/s RZ-OOK signals using wavelength conversion and chromatic dispersion," *Opt. Lett.* **34**(4), 542–544 (2009).

17. Y. Dai, X. Chen, Y. Okawachi, A. C. Turner-Foster, M. A. Foster, M. Lipson, A. L. Gaeta, and C. Xu, "1 microsecond tunable delay using parametric mixing and optical phase conjugation in Si waveguides," *Opt. Express* **17**(9), 7004–7010 (2009).
 18. E. Myslivets, N. Alic, S. Moro, B. P. P. Kuo, R. M. Jopson, C. J. McKinstrie, M. Karlsson, and S. Radic, "1.56-microsecond continuously tunable parametric delay line for a 40-Gb/s signal," *Opt. Express* **17**(14), 11958–11964 (2009).
 19. Y. Dai, X. Chen, Y. Okawachi, A. C. Turner-Foster, M. A. Foster, M. Lipson, A. L. Gaeta, and C. Xu, "1 μ s tunable delay using parametric mixing and optical phase conjugation in Si waveguides: reply," *Opt. Express* **17**(18), 16029–16031 (2009).
 20. S. R. Nuccio, O. F. Yilmaz, S. Khaleghi, X. Wu, L. Christen, I. Fazal, and A. E. Willner, "Tunable 503 ns optical delay of 40 Gbit/s RZ-OOK and RZ-DPSK using a wavelength scheme for phase conjugation to reduce residual dispersion and increase delay," *Opt. Lett.* **34**(12), 1903–1905 (2009).
 21. S. Namiki, "Wide-band and -range tunable dispersion compensation through parametric wavelength conversion and dispersion optical fibers," *J. Lightwave Technol.* **26**(1), 28–35 (2008).
-

1. Introduction

The ability to create precise all-optical delays, i.e., being able to control the arrival times of optical data streams on the physical level, is highly desirable in many areas such as communication networking [1], optical coherence tomography [2], optical control of phased array antennas for radio frequency communication [3], light detection and sensing [4], optical sampling [5], and pattern correlation [6]. Discrete optical delays, which can be generated by combining a series of fixed delay lines with different amounts of delay in parallel [7], are capable of a large range of discretely tunable delays with large granularity. However, a continuously tunable optical delay is required as the data rate increases since the time interval between adjacent bits is small. Recent research on continuously tunable optical delays includes the efforts to reduce the speed of light by several orders of magnitude (which is commonly known as "slow light") by utilizing a rapidly varying refractive index associated with nearby optical resonances, and delays of several pulse widths were obtained [8,9]. A larger tunable delay range is usually achieved by the "wavelength conversion and dispersion" delay scheme, which takes advantage of the group-velocity dispersion (GVD) in an optical fiber for generating a wavelength-dependent optical delay [10–20]. The wavelength of the input signal is first shifted and then injected into a medium with a large GVD, which generates a wavelength-dependent delay with respect to the initial signal pulse. The total delay is approximately the product of the GVD parameter, the length of the dispersive fiber, and the wavelength shift. As a result, large ranges of delay can be obtained by simply extending the fiber length or the wavelength conversion bandwidth. For example, with dispersion management using the wavelength-optimized optical phase conjugation [17], delay ranges larger than 1 μ s have been demonstrated experimentally without accumulating excessive residual GVD [17,18].

There are several limitations in extending the fiber length to further increase the tunable delay range. The increasing residual dispersion slope (which varies within the tuning range so that it cannot be fully compensated [17]) will impact the system performance, particularly at high data rates. The accumulated polarization mode dispersion (PMD) associated with the long fiber length eventually becomes too large for transmission at high data rates with acceptable fidelity. Furthermore, the significant fiber loss needs to be compensated by optical amplifications, which degrades the system optical signal-to-noise ratio (OSNR) and increases the delay line power consumption. It should be noted that 60 km of dispersion compensation fibers (DCFs) or more were used to achieve a 1- μ s delay range [17,18]. In comparison, a fixed 1- μ s delay can be generated by a standard single-mode fiber (SSMF) of 200 meters in length with negligible impact to the data fidelity, even at data rates of 100 Gb/s. Thus, the combination of discrete and continuously tunable delays can be an effective approach to achieve simultaneously fine, continuous tuning and an ultra-large delay range.

In this paper, we experimentally demonstrate the first continuously tunable optical delay line with extended delay range via a cascading discrete stage. Using a discrete stage with 16 wavelength-dependent delays and a continuously tunable stage capable of 711-ns delay range, we achieve a 7.34- μ s continuous tuning range. Four cascaded parametric four-wavelength mixing (FWM) stages in the silicon nanowaveguides are used in the system: one for the

discrete delay tuning, two for the continuous tuning with tunable dispersion compensation, and one for wavelength-preserving operation [11]. Using the wavelength-optimized optical phase conjugation scheme, zero residual GVD can be achieved throughout the tuning range. The bit-error-rate (BER) performance of the system is experimentally characterized using 10-Gb/s NRZ data.

2. System design and performance

The experimental setup and the principle of cascading the discretely tunable optical delay line and the continuous one are illustrated in Fig. 1.

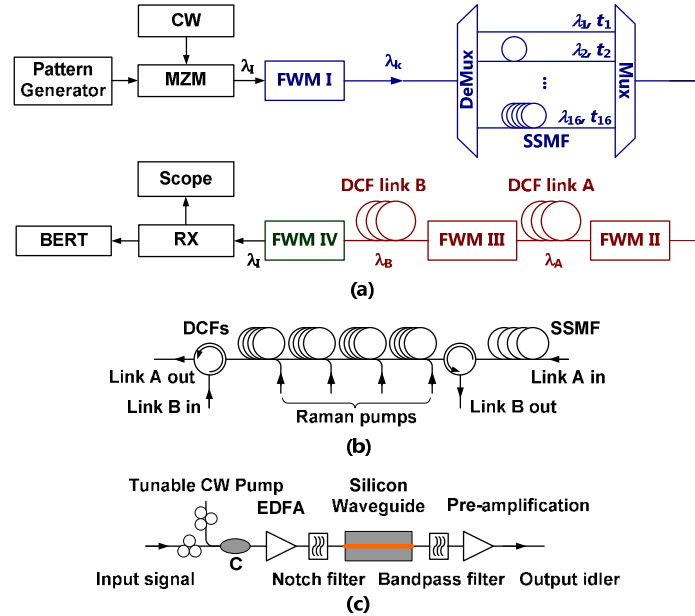


Fig. 1. (a) The experimental setup to cascade the discretely and continuously tunable delay line. (b) The setup for the two DCF links. Raman pumps are used in each DCF spools to fully compensate for the 40-dB propagation loss in the link throughout the wavelength conversion range. (c) The setup for each of the four wavelength conversion stages utilizing silicon waveguides.

A CW DFB laser centered at $\lambda_1 = 1563.5$ nm is modulated using a Mach-Zehnder modulator (MZM), generating the non-return-to-zero (NRZ) data as the input signal of the tunable delay system. The discrete stage, consisting of a pair of 200-GHz, 16-channel Mux / DeMux and 16 SSMFs with suitable lengths between them, provides a discrete tunable delay with very large granularity of hundreds of nanoseconds when its input wavelength is tuned among the 16 wavelengths by the first wavelength conversion. The length of the SSMFs in each discrete channel is measured by an oscilloscope at approximately 1-ns precision. The discrete delay stage is followed by a continuous tuning stage, containing the following two wavelength conversion elements and two DCF links, which provides a continuous tuning that is slightly larger than any of the delay steps between the adjacent discrete channels. As a result, a continuously tunable delay could be achieved without any gaps, and the total delay range of the continuous tuning is approximately the number of discrete channels multiplied by the maximal delay of the continuous stage. As shown in Fig. 1(b), four 15-km spools of DCF (HFDK, OFS Denmark) with a dispersion parameter of approximately -250 ps/nm/km are used as the two DCF links by using two circulators to form a double pass configuration. A 4-km SSMF spool is used before the first circulator to shift the dispersion curve of link A by approximately 65 ps/nm. Four broadband Raman pump modules are used to achieve lossless transmission in the DCF throughout the wavelength conversion range. A fourth wavelength

conversion is added after the continuous-delay module in order to realize the wavelength preserving operation. The system output is then detected by a standard 10-Gb/s receiver and evaluated by an oscilloscope and a BER tester (BERT). The four silicon-based FWM setups, shown in Fig. 1(c), are the same as those described in [17,19].

Tunable delays are obtained by tuning λ_k , λ_A , and λ_B , the three wavelengths in the discrete stage, link A, and link B, respectively, and k is the channel number. Note that the dispersion in the DCF links that generates the wavelength-dependent delay also distorts the signal. In addition, the phase distortion introduced by the SSMFs of the discrete stage can be significant for transmissions at high data rate. In order for the tunable delay system to support high data rate transmissions, our system is designed to achieve zero GVD at the final output throughout the delay tuning range. The residual GVD of the continuous stage, using the wavelength-optimized phase conjugating process [17,21], is used to compensate that of the discrete stage (see Fig. 2). λ_B is now determined by λ_k (discrete tuning) and λ_A (continuous tuning):

$$\chi_A(\lambda_A) - \chi_B(\lambda_B) = \chi_k \quad (1)$$

where χ_k is the dispersion of k th channel of the discrete stage, and $\chi_A(\lambda)$ and $\chi_B(\lambda)$ are the dispersion function for DCF links A and B, respectively. In our system, the requirement for a zero residual GVD [Eq. (1)] results in a 1- to 4-nm blue shift of λ_B from λ_A . Thus, by taking advantage of the tunable dispersion compensation enabled by the wavelength-optimized phase conjugation scheme, the second order dispersion of the SSMFs in the discrete stage can be fully compensated. In addition, high data rate transmissions could be supported by placing a fixed third-order-dispersion (TOD) compensator (e.g., a spool of dispersion shifted fiber) before or after the whole system. As shown in Ref. [17], the system performance with such a partial TOD compensation is only limited by the fourth-order dispersion of the fiber link.

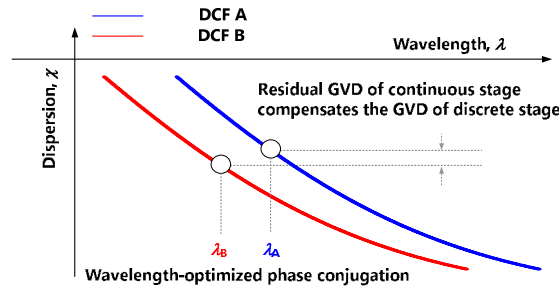


Fig. 2. Dispersion management scheme to achieve zero residual GVD for the entire delay system.

We performed both the discrete and the continuous wavelength tuning within the C-band of the EDFA, taking advantage of the mature and low-cost optical devices (e.g. filters and amplifiers) within this band. The wavelength conversion ranges of the two stages overlap since 16 200-GHz channels cover a large portion of the C-band. Due to the requirement to spectrally separate the idler from the signal and the pump in each of the FWM stages, there should be a minimum wavelength separation between the signal and the idler. As a result, the wavelength λ_k of the k th channel in the discrete stage should not overlap with the wavelength tuning range of the continuous stage when the k th channel is used. Otherwise there would be a gap in the tunable delay since λ_A cannot be tuned continuously in the vicinity of λ_k . In our design, we confine the tuning range of λ_A within either the blue side or the red side of λ_k , depending on which side provides a larger continuously tunable delay range. The wavelength ranges used in the experiment are shown in Fig. 3(a) (colored lines). By compromising the maximum delay range, we achieve both the discrete and the continuous tuning within the C-band.

The total delay of the entire system is simply the sum of the discrete part and the continuous part, see Eq. (2). According to [17] the delay in the continuous stage can be

expressed in terms of the wavelengths λ_A and λ_B , and the dispersion functions $\chi_A(\lambda)$ and $\chi_B(\lambda)$ for DCF links A and B, respectively. The delay in the discrete stage, τ_{discrete} , is determined by the fiber length in each channel. The total delay of the system is then

$$\tau(k, \lambda_A, \lambda_B) = \tau_{\text{discrete}}(k) + \left[\int_{\lambda_{A,1}}^{\lambda_A} \chi_A(\lambda) d\lambda + \int_{\lambda_{B,1}}^{\lambda_B} \chi_B(\lambda) d\lambda \right] \quad (2)$$

where $\lambda_{A,1}$ and $\lambda_{B,1}$ are the reference wavelengths (the starting points of the wavelength conversion ranges when the 1st channel of the discrete stage is used) in DCF links A and B, respectively, i.e., $\tau(k=1, \lambda_A = \lambda_{A,1}, \lambda_B = \lambda_{B,1}) = 0$. Equation (2) can also be expressed explicitly in terms of the starting wavelengths in the DCF links when the k th discrete channel is selected.

$$\tau(k, \lambda_A, \lambda_B) = \tau_{\text{discrete}}(k) + \left[\int_{\lambda_{A,1}}^{\lambda_{A,k}} \chi_A(\lambda) d\lambda + \int_{\lambda_{B,1}}^{\lambda_{B,k}} \chi_B(\lambda) d\lambda \right] + \left[\int_{\lambda_{A,k}}^{\lambda_A} \chi_A(\lambda) d\lambda + \int_{\lambda_{B,k}}^{\lambda_B} \chi_B(\lambda) d\lambda \right] \quad (3)$$

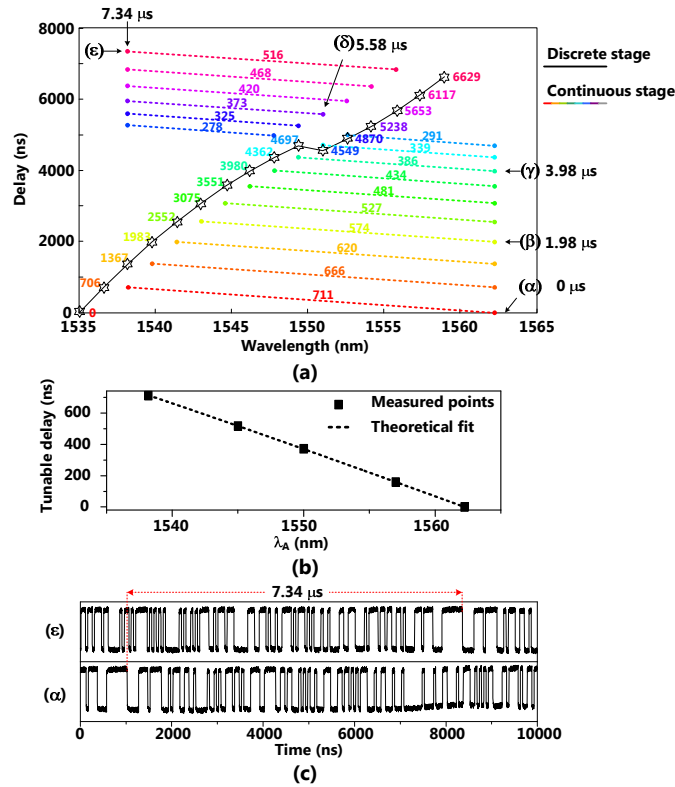


Fig. 3. (a) The tunable delay values in terms of the discrete (λ_k , black line) and the continuous (λ_A , colored lines) wavelength tunings. \star points indicate the positions for the 16 discrete channels: the wavelengths and the delay values. The colored lines show the wavelength tuning and the delay range of the continuous stage when the corresponding discrete delay is chosen. (b) Measured tunable delay of the continuous stage as a function of λ_A when the 1st channel is chosen. The delay is measured directly by an oscilloscope with a data pattern at 100 Mb/s. (c) The measured 7.34- μ s delay between the shortest delay setting at (α) and the longest delay setting at (ϵ). A data pattern at 20 Mb/s is used for the measurement.

$\lambda_{A,k}$ and $\lambda_{B,k}$ are the starting points (longest wavelengths) of the wavelength conversion ranges in DCF links A and B, respectively, when the k th channel is used. The values of the continuous delay tuning within each discrete channel (represented by the third term in Eq. (3) [17]) are measured and indicated in Fig. 3(a) (the values above the colored lines). In

particular, the measured tunable delay for the 1st channel, which has the largest wavelength tuning range, as a function of λ_A is plotted in Fig. 3(b), showing a total delay range of 711 ns. The step of the discrete delay [the first two terms in Eq. (3)] is designed to be 4 to 5 ns less than the corresponding continuous tuning range, ensuring continuous tuning between two adjacent discrete channels. For the entire system, the delay values at five points, as shown from (α) to (ϵ) [see labels in Fig. 3(a)], are measured. As shown in Fig. 3(c), the combined discrete and continuous stages provide a tunable delay range of 7.34 μ s, which is significantly larger than previous experiments that use continuous stage only [17,18].

It is interesting to note that the discrete delays include two contributions: (1) the discrete delay introduced by the SSMF [τ_{discrete} , the first term in Eq. (3)], and (2) a channel offset due to the variations in the starting wavelengths of the continuous stage [the second term in Eq. (3)]. Since the last 6 discrete channels have starting points other than $\lambda_{A,1}$, the channel offsets are nonzero for $k > 10$. As shown in Fig. 3(a), these channel offsets were taken into account by shortening the SSMFs accordingly for delay channels 11 through 16.

3. System BER performance at 10 Gb/s NRZ data

We measured the BER performance of the entire system after four parametric processes using a 10 Gb/s NRZ data channel with a $2^{31}-1$ PRBS sequence. Five delay points, from (α) to (ϵ) as shown in Fig. 3(a), are measured. Figure 4 shows the optical spectra of the four silicon-based FWMs when the γ point is measured.

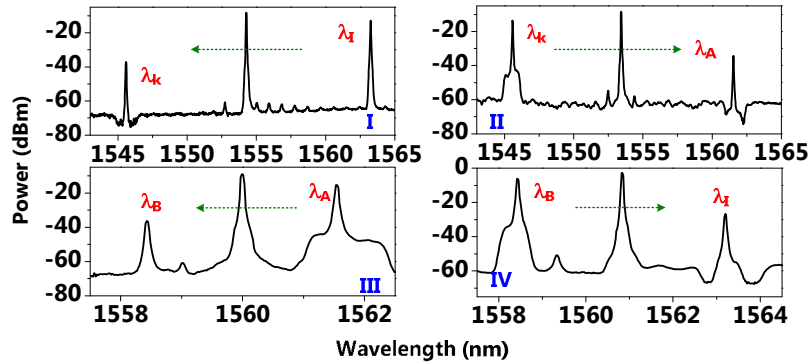


Fig. 4. Optical spectra of the four FWMs for achieving the delay value at the γ point. Arrows show the wavelength conversion directions.

Although the wavelength conversion efficiency in current silicon waveguides is not high, at approximately -20 dB on-off conversion efficiencies (i.e. the ratio of the idler power to the signal power at the output of a waveguide, as shown in Fig. 4) in our experiment, good OSNRs of the idler waves can be achieved after the FWM process by using notch filters before the Si-waveguides, which eliminate the ASE noise at the spectral regions where the idlers will be generated [17] (the spectral feature of the notch filter in Fig. 4 III is masked by the converted noise pedestal of the signal band since the bandwidth of the notch filter in Fig. 4 III is less than those used in the other figures). Figure 5 shows the BERT results of the five measured points after the whole system with four cascading wavelength conversion stages. The measured power penalty is 3.7 to 4.3 dB at a BER of 10^{-9} . Our experiment demonstrates that all four wavelength conversion processes can be accomplished using the Si nanowaveguides.

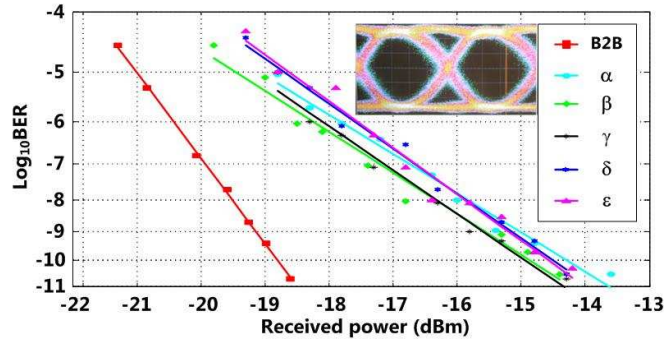


Fig. 5. Measured BER curves of back-to-back (B2B) and after transmission through the entire tunable delay systems at different delays. Insert shows the eye-diagram measured at γ delay at a BER of less than 10^{-11} .

4. Conclusion

We demonstrated an all-optical, continuously tunable parametric delay system by cascading the discrete and the continuous tuning stages. A large continuous tuning range of $7.34 \mu\text{s}$ is achieved. The wavelength-optimized optical phase conjugation scheme was used to minimize the residual dispersion of the system, making the delay system capable of high data rate transmission. Four successive wavelength conversions were performed using silicon waveguides. The system BER performance was measured for 10 Gb/s NRZ data with a power penalty of 3.7 to 4.3 dB.

Acknowledgments

The authors gratefully acknowledge support from the DARPA MTO POPS Program. This work was performed in part at the Cornell NanoScale Facility, a member of the National Nanotechnology Infrastructure Network, which is supported by the National Science Foundation. We also acknowledge valuable discussions with Prof. Keren Bergman and her research group at Columbia. OFS Denmark is acknowledged for loaning parts of the HFDK.